Intrinsic defects and krypton impurity atoms in hcp titanium: A first-principles study

Abdulrafiu T. Raji,[1,*] Riccardo Mazzarello,[2] Sandro Scandolo,[3,4] Schadrack Nsengiyumva,[1] Margit Härting,[1] and David. T. Britton[1]

[1]*Department of Physics, University of Cape Town, Private Bag X3, Rondebosch, Cape Town 7701, South Africa*

[2]*Institut für Theoretische Festkörperphysik and JARA–Fundamentals of Future Information Technology, RWTH Aachen University, D-52056 Aachen, Germany*

[3]*Abdus Salam International Centre for Theoretical Physics, Strada Costiera 11, I-Trieste 34151, Italy*

[4]*INFM/Democritos National Simulation Centre, via Beirut 2-4, I-Trieste 34151, Italy*

We report on the migration of monovacancies, divacancies, and substitutional krypton atoms in hcp titanium using the nudged elastic band method, in the framework of *ab initio* density functional theory. The divacancy migration energy barrier is found to be lower than that of a monovacancy. The migration of substitutional krypton in titanium is governed by the vacancy mechanism, if there is an excess of nonequilibrium vacancies after the implantation. However, if thermal vacancies dominate, krypton atom migration is expected to proceed via the dissociation mechanism. We also present *ab initio* calculations on the formation of clusters of multiple substitutional impurity krypton atoms and the interactions between krypton impurities and vacancies in titanium. We have found that, analogous to multiple interstitial krypton clusters, clusters of substitutional krypton atoms are energetically unstable, but are stabilized by vacancies. However, the efficiency of stabilization by vacancies depends strongly on the spatial distribution of the vacancies within the clusters. This study indicates the possibility of inert gases to nucleate in voids created by vacancies in ion implantation processes.

PACS number(s): 61.72.−y

I. INTRODUCTION

Noble-gas atoms introduced into metals by ion implantation, or by nuclear reaction processes, are insoluble and agglomerate into nanometric-sized precipitates.[1,2] To study the properties of inert-gas atoms in metals, one can exploit the tendency of energetically injected atoms, e.g., by ion implantation, to cluster together with lattice defects such as vacancies and to form nanometric-sized bubbles.[3] A spherical bubble in thermal equilibrium will be under a pressure given by $P = 2\gamma/r$, where γ is the interfacial free energy and r is the radius of the bubble.[4] Therefore, for very small radii, of the order of nanometers, this yields gigapascal pressures in an implanted material. Thus, compression of noble-gas particles by metal matrices allows room-temperature investigations of pressure effects without resorting to complex high-pressure equipment. In nuclear reactors, the mechanical properties of metallic fuel elements are degraded by the production of self-defects, as well as diffusion and clustering of rare-gas atoms into bubbles, which leads to a macroscopic swelling of the fuel or its cladding.[5] Also, electrical properties of metals have been shown to be affected by the presence of implanted noble-gas atoms.[6]

There is a wealth of experimental studies on the behavior of noble-gas elements in metals, in particular, cubic metals.[7–10] In the past decade, the advent of high-resolution transmission electron microscopy (HRTEM) has rekindled interest in the structural characterization of noble-gas nanoparticles embedded in a metal matrix.[1] Apart from experiments, electronic structure calculations based on density-functional theory (DFT)[11,12] have helped to elucidate the properties of impurity noble-gas atoms in metals. In recent times, *ab initio* DFT calculations of energetics of helium atoms in cubic metals have been reported.[13–15] The motivation for these studies is the need to understand the fundamental behavior of helium atoms

in metals, with a view to elucidate how their formation and dynamics affects the mechanical stability of nuclear materials.

The work presented in this paper concerns the migration of krypton and self-defects (vacancies and divacancies), and the formation of krypton-vacancy complexes in krypton-implanted hcp titanium. In our previous study,[16] we reported the tensile stress relaxation effect of an implanted krypton atom in hcp titanium. We adduced the relaxation in the near surface ($\sim$100 nm) stress to the creation, migration, and clustering of point defects in titanium. Open volume defects (vacancies and their clusters) were monitored using positron annihilation lifetime spectroscopy (PAS).[16] It was observed that deeper in the material, beyond the projected range of krypton implantation, point defects agglomerate to form larger defect structures that introduce additional compressive stress. Therefore, this study has been partly motivated by the need to identify possible defect configurations, and migration mechanisms leading to the formation of defect complexes in hcp titanium.

Compared to cubic metals, there have been far fewer studies on hexagonal metals. This study therefore contributes to the understanding of the migration of point defects in the latter. In addition, it will provide theoretical evidence for the existence of gas-filled cavities in metals energetically injected with inert-gas atoms. Inert-gas inclusions in a cavity may exhibit unusual optical and electronic properties.[1] Furthermore, the presented results might be of relevance to the field of semiconductor nanostructures,[17] where there is need to reduce high internal stresses. Point defects migrate under the influence of stress, and they play important roles in the degradation or failure of metallic interconnects in semiconductor devices[18] and clustering of radiation damage-induced defects.[19]

All calculations in this work have been performed in the framework of DFT, using the plane-wave pseudopotential (PP)

approach.[20] The paper is organized as follows: In Sec. II, we discuss the methodology of the calculations. In Sec. III A, we present results on migration mechanisms for monovacancies, divacancies, and substitutional krypton, calculated using the nudged elastic band method (NEB).[21] Monovacancy migration dominates diffusion in metals at ordinary temperature, however, at high temperatures divacancy migration may be significant.[22] This is particularly relevant in ion implantation processes where the implantation-affected region experiences a very high local temperature, close to the melting temperature of the host material, in a process known as thermal spike.[23,24]

Energetics of substitutional krypton-vacancy defect clusters is presented in Sec. III B. Our justification for considering such defect complexes is the following: It has been shown theoretically that crystal lattice vacancies migrate and agglomerate in the form of clusters in metals,[25] and that noble-gas atoms, when energetically injected into metals, cluster with lattice vacancies to form bubbles.[3,26] Furthermore, using the PAS experimental technique, we observed the presence of vacancy clusters in krypton-implanted titanium, and the implanted krypton atom profile was determined using Rutherford backscattering spectroscopy.[16] The presence of vacancies results from atomic collisions between injected krypton atoms, introduced via the ion implantation, and titanium lattice atoms.[16] The injected krypton atoms may occupy different crystallographic sites. However, in our previous theoretical study,[27] we found that the substitutional site is the most energetically favorable. Hence, defect complexes in the form of substitutional krypton-vacancy clusters are possible. Moreover, such defect complexes have been postulated to serve as the nucleation center for inert-gas precipitates introduced via ion implantation, and their shapes and atomic structures are the subject of ongoing studies.[1,28]

In Sec. III C, we examine the energy landscapes of substitutional krypton migration, via the vacancy mechanism. This is particularly relevant because the growth of the inert-gas precipitates is dependent on the motion and agglomeration of vacancies and inert gas inclusions.[29] A brief summary of our major findings is given in Sec. IV.

II. METHODOLOGY

All the first-principles calculations were carried out using the plane-wave self-consistent field (PWSCF) code, included in the QUANTUM ESPRESSO (QE) package,[30,31] which implements the DFT, using the plane-wave pseudopotential method.[20] The exchange-correlation potential is described by the generalized gradient approximation (GGA), as developed by Perdew and Wang (PW91).[32] For titanium, we used an ultrasoft pseudopotential (USPP) of the Vanderbilt type[33] that includes $4s$ and $3d$ states and the semicore states ($3s$ $3p$) in the valence band. For krypton atoms, we used an USPP having $4s$ and $4p$ electrons in the valence band. The pseudopotential for titanium is taken from the existing QE library, while we generated the USPP for krypton. Regarding the cutoff energy for the plane-wave basis set, we performed extensive convergence tests with values up to 45 Ry, but convergence with respect to the total energy, within 10^{-3} Ry per atom, was achieved with 35 Ry. Hence this cutoff energy value was used throughout the study. In addition, convergence of the total energy of bulk titanium to within 10^{-3} Ry per atom with respect to the

discrete Brillouin zone (BZ) sampling was achieved for an $8 \times 8 \times 8$ k-point mesh, while equivalent meshes were chosen for supercell structures. The BZ integration was performed using the Methfessel-Paxton scheme,[34] with a smearing width $\sigma = 0.02$ Ry. The physical properties of hcp titanium calculated with these parameters were presented in our earlier study.[35] The calculations of the formation energies and migration energies of vacancies were repeated using a smaller width, $\sigma = 0.005$ Ry, to check how they depend on this parameter: it was found that the new values of the energies differ by 0.1 eV or less from those obtained by employing $\sigma = 0.02$ Ry and that the relative values of the migration energies do not change significantly.

Mono- and divacancy migration has been studied using the climbing image NEB (CI-NEB) method,[21] as implemented in QE. This is an efficient method for finding the minimum energy path (MEP) when the initial and final state of a transition process are known, and can be used to estimate the migration energy barrier between two equilibrium states. Within this method, the MEP is found by optimizing a number of images between the initial and the final states, along the reaction path. There are two paths for monovacancy migration in a hcp structure: the *in plane* and the *out of plane.* These are shown in Fig. 1(a) and have been denoted as B_v and A_v, respectively. As far as divacancies are concerned, we have previously shown[34] that first- and second-neighbor divacancies are thermodynamically stable, and *out-of-plane* divacancies have slightly lower energy than *in plane* divacancies. For the divacancy migration, a total of four migration paths have been considered. These have been denoted as D_{ab}, D_{aa}, D_{ba}, and D_{bb} and are shown in Figs. 1(b) and 1(c). The divacancy migration is such that one of the vacancies rotates about the other. On completion of the rotation, the divacancy either preserves its initial configuration or transforms into the other. For example, the migration path denoted as D_{bb} is such that the two vacancies remain in the same plane, on completion of the migration. Similarly, the D_{aa} migration on completion of its path retains its configuration. On the other hand, in the case of D_{ba}, the migrating vacancy moves to the next atomic plane (along the c direction) and the initial divacancy configuration therefore changes from two vacancies in the same atomic plane (separated by the lattice parameter a) to two vacancies now oriented along the c direction. Also, for the D_{ab} migration path, a vacancy moves from an adjacent atomic plane (along the c direction) such that the two vacancies are now separated by the equilibrium lattice constant a, in the same atomic plane. The initial divacancy configuration therefore changes, and divacancy diffusion may proceed further via *in-plane* vacancy migration.

The monovacancy and divacancy MEPs have been calculated using 48 and 64 atomic sites supercells, respectively. The dimensions of the supercells are $3a \times 2a\sqrt{3} \times 2c$ and $4a \times 2a\sqrt{3} \times 2c$. These cell sizes have been shown[35] to be sufficient for convergence of the formation energies of monovacancy and the two divacancy configurations, respectively. Using larger supercells was found to affect the calculated formation energy by less than 0.02 eV. For a single-vacancy migration, a total of five images have been used, while seven images were used for determining the MEP and the activation energy barrier for the divacancy diffusion. The MEPs for the two migration
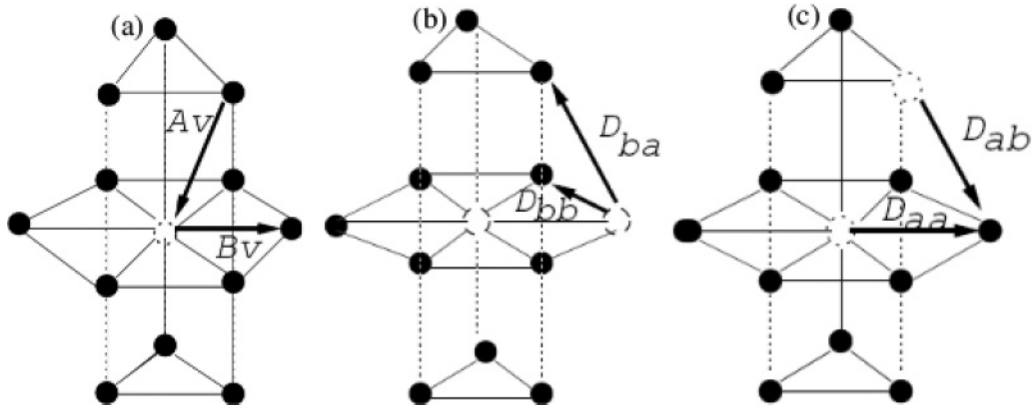
FIG. 1. Schematics of monovacancy and divacancy migration in hcp titanium lattice: (a) in-plane (B_v) and out-of-plane (A_v) monovacancy migration, (b) possible rotations of basal (in-plane) divacancy, and (c) possible rotations of out-of-plane divacancy. Black filled circles represent titanium atoms, while open circles stand for vacancies.

processes proposed for the substitutional krypton were also investigated using the CI-NEB method. Supercells containing 63 atomic sites (62 titanium atoms plus a krypton atom), a k-point grid of $2 \times 2 \times 2$, and a cutoff energy of 35 Ry were used. It was observed that a denser k point, such as a $2 \times 2 \times 3$ mesh, does not affect the barrier energy by more than 0.03 eV and has no effect on the MEP. Results on the relative stabilities of single krypton defects in hcp titanium in substitutional and two interstitial sites have been presented in Ref. 27. Here we focus on possible clusters of substitutional krypton atoms and vacancies. The interaction energy between vacancy and krypton clusters in a supercell containing N titanium atoms can be defined as[36]

$$\delta E_{\text{int}}(v - \text{Kr}) = E(v_n - \text{Kr}_p) + E_N(\text{Ti}) - E(v_n) - E(\text{Kr}_p). \quad (1)$$

Here, the first term on the right-hand side is the total energy of an atomic system consisting of n vacant sites (denoted by v) and p near-neighbor sites of the vacancies occupied by krypton atoms, all remaining sites being titanium atoms. The second term, $E_N(\text{Ti})$, is the energy of a perfect hcp titanium lattice containing N lattice sites, while $E(v_n)$ is the energy of a titanium lattice containing n vacancies. The last term, $E(\text{Kr}_p)$, is the energy of the supercell containing p krypton atoms in p substitutional sites. Simulation cells of dimension $4a \times 5a \times 3c$ containing 120 titanium atoms were used for the calculations, while allowing the relaxation of the atomic coordinates at fixed supercell shape and volume. In Eq. (1), a negative interaction energy indicates an attraction, while a positive energy indicates repulsion between the vacancies and the krypton atoms making up the configurations.

A large number of different krypton (Kr)-vacancy (V) defect cluster configurations pKr-nV, where p is the number of krypton atoms and n is the number of vacancies, has been investigated in this study (see Fig. 2). Defects 2 and 3 in Fig. 2 correspond to two different combinations of 1Kr and 1 vacancy. For $p = 2$, a systematic investigation of the energetics of compact configurations (where each vacancy interacts maximally with at least one Kr atom) with $n = 0$, 1, 2, 3 was carried out. In the following, we will discuss only

the three most stable defects for each pKr-nV pair with $p = 2$ and $n = 0, 1, 2, 3$ (these configurations are shown in Fig. 2) and compare their interaction energies. Three clusters with $p = 2$ and $n = 4$ were also considered in order to assess how the spatial distribution of vacancies determines the binding energy. Thus, defects 4–6 are 2Kr-0V ($p = 2$; $n = 0$) clusters, defects 7–9 are 2Kr-1V ($p = 2$; $n = 1$) clusters, defects 10–12 are 2Kr-2V ($p = 2$; $n = 2$) clusters, and so on. We also studied larger clusters consisting of $p = 10$, $n = 1, 7, 9$, as well as $p = 11$, $n = 0$ krypton-vacancy combinations. There are obviously many more possible arrangements of vacancy-krypton atoms in the form of defect complexes in the titanium matrix. However, these configurations have been selected in order to obtain information about energetic trends and the interplay between the presence of vacancies, their spatial distribution with respect to krypton atoms, and the relative stability of substitutional krypton-vacancy clusters in titanium. Such information is crucial in understanding the stress relaxation effects of defects created via krypton ion implantation in titanium.[24] In addition, some of the defect models will enable us to examine the possibility of inert-gas-filled voids in krypton ions implanted titanium.

The description of the defect configurations is as follows: defect configuration 1 is a simple substitutional krypton; defect 2 consists of a vacancy and a substitutional krypton at the nearest possible distance; defect configuration 3 consists of a substitutional krypton atom and a vacancy in the same plane, separated by lattice parameter a; configuration 4 is two krypton atoms placed at the nearest possible distance; defect 5 is two krypton atoms in the same plane separated by a; defect 6 is two krypton atoms separated by $2a$ with a titanium atom in the middle of separation, i.e., at distance a from either of the krypton atoms; defect 7 is made of two substitutional krypton atoms and a vacancy in the same plane such that they form a triangle pattern; defect 8 is similar to 6, because the two krypton atoms are separated by distance $2a$, but the titanium atom located midway between the two krypton atoms is now replaced with a vacancy; defect 9 consists of a vacancy in an atomic plane and two krypton atoms in a plane above, such that each of the krypton atoms is equidistant from the vacancy; defect 10 is two krypton atoms in the same plane, separated

(0001) plane ——→

$\langle\bar{1}\bar{1}20\rangle$

$\langle\bar{1}2\bar{1}0\rangle$
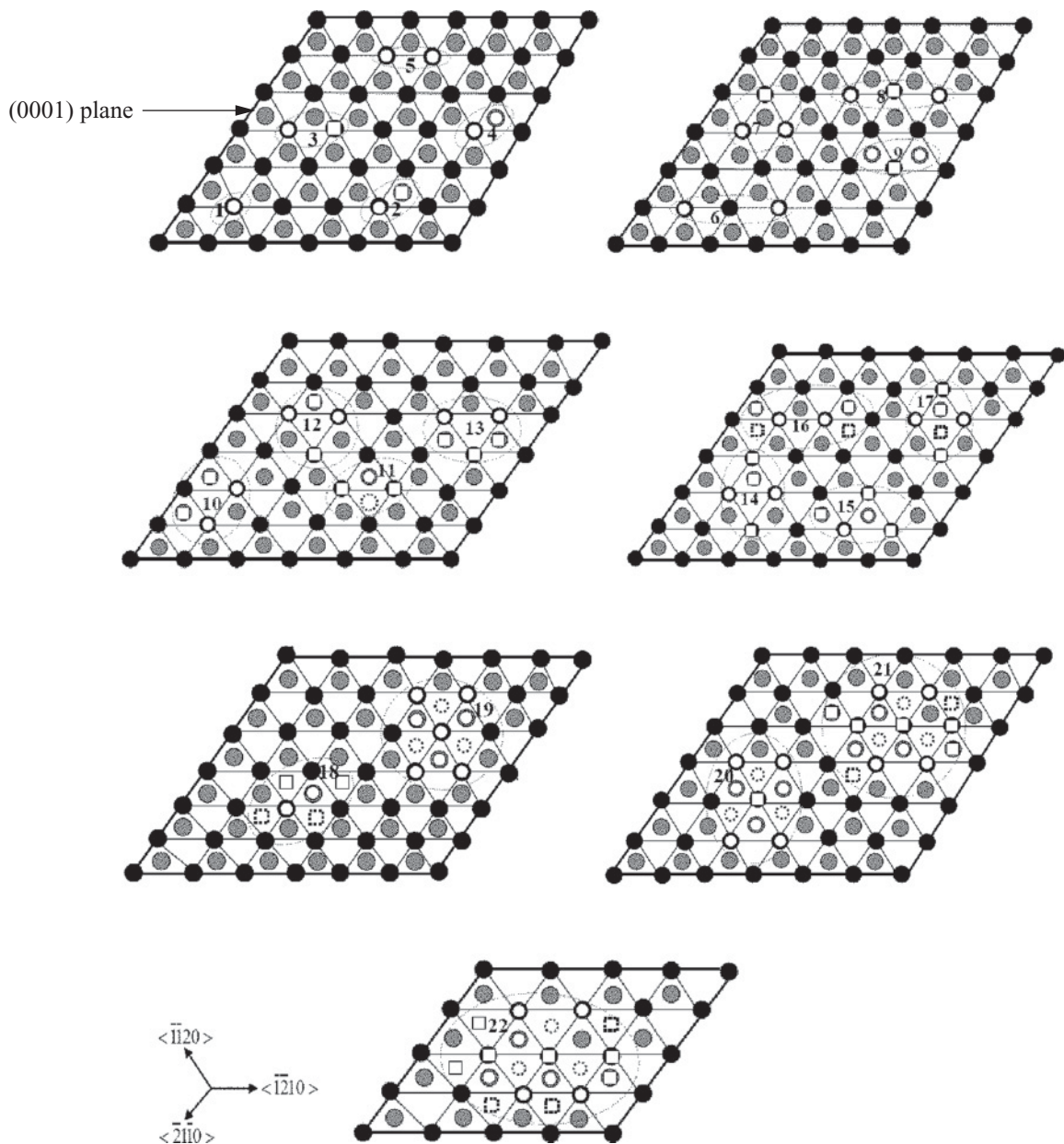
$\langle\bar{2}\bar{1}\bar{1}0\rangle$

FIG. 2. Different arrangements of substitutional-krypton and vacancy clusters in titanium, as described in the text. Black circles represent titanium atoms in the (0001) plane; gray circles are titanium atoms above the plane; open circles and open rectangles are, respectively, krypton atoms and vacancies; dotted circles and dotted rectangles, respectively, represent krypton atoms and vacancies below the plane. For proper identification, each defect cluster has been enclosed and labeled with numbers 1–22.

by a, and two vacancies in the plane above the krypton plane, such that each of the vacancies is at the closest distance to a krypton atom; defect 11 is similar to 10 except that the two vacancies are positioned such that each of the krypton atoms is at the nearest distance to the two vacancies; in the case of defect 12, two krypton atoms and a vacancy form an equilateral triangle of side a in a plane, and a vacancy equidistant to each of the krypton atoms is positioned at the next plane above. Each of defects 13–15 consists of two krypton atoms and three vacancies. Defect 13 is similar to 12, except that, instead of a vacancy above the triangular plane, there are now two vacancies such that each of the vacancies is at the closest

possible distance to each of the krypton atoms. In defect 14, two krypton atoms and two vacancies form a parallelogram in a plane and the third vacancy is at equidistant position from a triangular half of the parallelogram. In defect 15, two krypton atoms are positioned in separate planes, such that they are at the nearest possible atomic positions. In this cluster, there are two vacancies on the same plane, with one of the krypton atoms and one vacancy on the same plane with the other krypton. Defect configurations 16–18 have four vacancies and two krypton atoms. In the case of defect 16, the two krypton atoms are separated by a, and there are two vacancy pairs arranged in such a way that each pair is at the nearest equidistant positions

to each of the krypton atoms. Defect 17 is similar to 16, but in the former, the four vacancies are positioned such that they are at the closest possible distances to the krypton atoms. Defect 18 consists of two krypton atoms positioned diagonally at the nearest atomic sites. The four vacancies are positioned such that there are two vacancies in an atomic plane above one of the krypton atoms and the other two vacancies in a plane below the other krypton atom. Defect 19 is made up of 11 krypton atoms in substitutional sites arranged in the closest possible way, and it has no vacancy. Defect 20 is similar to 19 except that the central krypton atom in the latter is now replaced with a vacancy in the former. Finally, each of the defects 21 and 22 contains ten krypton atoms. In the former, however, seven vacancies make up the krypton-vacancy configuration while nine vacancies make up the configuration in the latter. The krypton-vacancy arrangements are such that they are at the closest possible distances.

III. RESULTS AND DISCUSSION

A. Vacancy migration

The calculated physical properties of pure hcp titanium have been presented in our previous work.[35] It is sufficient to mention here that they are in good agreement with available experimental data.

Ab initio studies of vacancy migration in hcp metals are rare.[37] The present study aims at providing insights into possible diffusion mechanisms for open volume point defects in a hcp metal. Figure 3(a) shows the MEPs for the *in-plane* and *out-of-plane* vacancy migration. In Table I, we show the initial and final coordinates of the migrating atoms, the positions of the saddle points, and the barrier energies for monovacancy migration. A significant anisotropy is found for the migration of a single vacancy with migration barrier energies of $E_{mi}^v = 0.47$ eV and $E_{mo}^v = 0.61$ eV, for the in-plane and out-of-plane migrations, respectively. This indicates that in-plane migration is preferred, in agreement with the experimental results of Hood,[38] where it was suggested that vacancies might diffuse faster in the basal plane than along the c direction.[39]

Results from theoretical calculations of self-diffusion properties in hcp metals are very sensitive to the type of interatomic potential employed. The embedded atom method (EAM) studies by Zope[40] slightly favored in-plane basal migration in hcp titanium, whereas Fernández,[41] also using two different types of EAM interatomic potentials, reported 0.51 (0.48) eV and 0.65 (0.65) eV, respectively, for the in-plane (out-of-plane) vacancy migration energy barrier in hcp titanium, thus slightly favoring out-of-plane migration. EAM many-body potential studies of Hu *et al.*[23] also predicted 0.61 (0.56) eV for the in-plane (out-of-plane) single-vacancy migration. However, EAM potentials are usually fitted so as to reproduce equilibrium physical parameters of materials such as elastic constants, the lattice spacing, or the c/a ratio, as in the case of hcp metals. On the other hand, single-vacancy migration involves atoms that are much closer to one another than the equilibrium distance during the diffusion process. Therefore, EAM potentials offer simplified descriptions of the real situation occurring in diffusion processes, and migration properties predicted by such potentials may therefore be inaccurate.
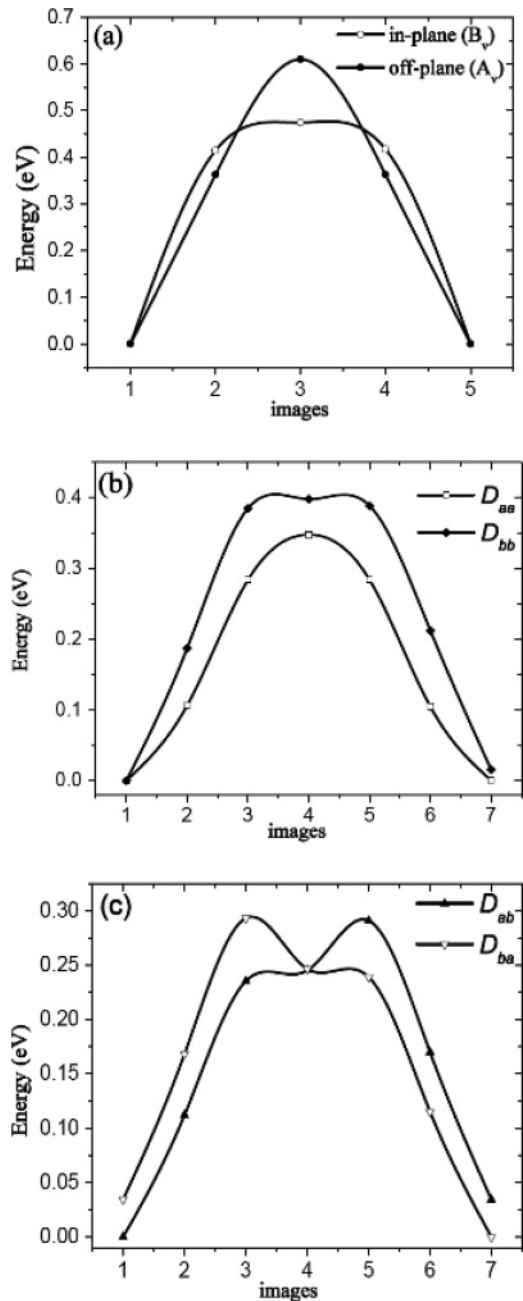

FIG. 3. Energy profiles for vacancy and divacancy migration: (a) vacancy migration, (b) and (c) divacancy migration.

Ab initio calculations, on the other hand, are in principle more accurate and provide a better description of interactions between atoms at both equilibrium and nonequilibrium positions. The knowledge of the migration energy barrier E_m^v allows us to estimate the activation energies for self-diffusion h_s^{sd}, defined as[40,41] $E_m^v + E_f^v$ (E_f^v is the vacancy formation energy), and then compare with values obtained from experiments. Using $E_f^v = 1.92$ eV,[21] $h_{si}^{sd} = 2.39$ eV and $h_{so}^{sd} = 2.53$ eV for the in-plane and out-of-plane vacancy migration, respectively. Our calculated results for the activation energy do not agree well with those reported in experiments. Both Libanati *et al.*[42] and Köppers *et al.*[43] reported $h_{so}^{sd} = 1.27$ eV and $h_{si}^{sd} = 3.14$ eV, respectively. As regards previous theoretical studies using

TABLE I. Initial and final defect orientation in vacancy and divacancy migration. Also shown are the positions of interstitial (saddle) point locations. Migration barrier energies (in eV) are shown as well. For each of the divacancy migration jumps, the asterisk ($*$) indicates the coordinates of the migrating atom, while the other coordinate is for fixed vacancy. Double asterisks ($**$) are the estimates of the migration energy barriers for the divacancy diffusion paths, obtained by considering two saddle points for each path, as explained in the text.

Defect	Migration jump	Interstitial location	Migration barrier (eV)
Vacancy	$B_v(0,0,0) \rightarrow (a,0,0)$	$0.34a, 0.05a, 0$	0.47
	$A_v(0,0,0) \rightarrow (a/2, -a/2\sqrt{3}, c/2)$	$a/2, -a/4\sqrt{3}, c/4$	0.61
Divacancy	$D_{aa}: (0,0,0) \rightarrow (a,0,0)^*$	$0.5a, 0.67a, 0.01c$	0.35
	$(a/2, -a/2\sqrt{3}, c/2)$		
	$D_{ab}: (0,0,0)$	$0.69a, -0.01a, 0$	0.24**, 0.29 **
	$(a/2, -a/2\sqrt{3}, c/2) \rightarrow (0,0,a)^*$		
	$D_{bb}: (0,0,0) \rightarrow (a,0,0)^*$		0.40
	$(a/2, -a\sqrt{3}/2, 0)$		
	$D_{ba}: (0,0,0)$		0.20**, 0.25**
	$(0,0,a) \rightarrow (0, -a/2\sqrt{3}, c/2)^*$		

interatomic potentials, $h_{si}^{sd} = 2.31$ eV,[44] 2.77 eV,[45] and $h_{so}^{sd} = 2.16$ eV,[44] and 2.77 eV (Ref. [45]) have been reported.

Divacancy migration is more complex. The initial and the final coordinates of the divacancies, the saddle-point coordinates, and the migration energy barriers for four different types of divacancy migrations are also shown in Table I. For the D_{aa} and D_{bb} migration, the saddle point is obvious and the migration energy barriers are $E_{aa}^d = 0.35$ eV and $E_{bb}^d = 0.40$ eV. The MEP paths are shown in Fig. 3(b). The MEPs for the D_{ab} and D_{ba} migrations are shown in Fig. 3(c). Images 5 and 3 for the D_{ab} and D_{ba}, respectively, correspond to the saddle points, and their configurations are such that the migrating atom is at the center of an equilateral triangle formed by three nearest-neighbor atoms. The migration energy barriers are $E_{ab}^d = 0.29$ eV and $E_{ba}^d = 0.25$ eV, respectively. Image 4 for both divacancy migrations corresponds to three nearest-neighbor vacancies with the diffusing atom located at the center of the triangle. This configuration has been described as the saddle point by Johnson.[44] If this image is taken as the saddle point, the migration energy barrier for the D_{ab} and D_{ba} configurations are, respectively, $E_{ab}^d = 0.24$ eV and $E_{ba}^d = 0.20$ eV. The choice of the appropriate saddle points is best resolved by carrying out a vibrational analysis[46] of the configurations corresponding to the images. Nevertheless, with the present results, we may already conclude that divacancy migration is faster than single-vacancy migration, and that divacancy migration is such that the two vacancies move between two nearest planes in the c direction. The finding that the divacancy diffusion energy barrier is lower than that of a monovacancy is not entirely surprising, because similar results were obtained for copper[47,48] and titanium[23] in previous theoretical studies using the EAM approach. The lower divacancy migration barrier may be explained by the following physical mechanism: Divacancy diffusion in an hcp lattice is such that one of the vacancies rotates and the other maintains its initial position [Figs. 1(b) and 1(c) and Table I]. However, the nonmigrating vacancy may act such that it relaxes the first nearest neighbors to the jumping atom when at the saddle points. Thus, the diffusing atom (when at the saddle points) experiences less

resistance to its migration, and less energy is therefore required to overcome the barrier. This is in contrast to the monovacancy diffusion (A_v or B_v) mechanism, because the relaxation of the nearest-neighbor atoms at the saddle point is owing only to the exchanging atom. The atom thus experiences more resistance to its migration, and the migration energy barrier is therefore higher than that of a divacancy.

B. Relative stabilities of krypton-vacancy clusters

In Table II, we summarize the results for the interaction energies obtained for the defects configurations shown in Fig. 2. The interaction energies have been calculated using Eq. (1). The second and the third columns in Table II list, respectively, the number of vacancies (n) and the number of krypton atoms (p) making up each of the clusters, while the fourth column gives the interaction energy per krypton atom for each of the defects. The first conclusion to be drawn is that multiple substitutional krypton clusters, without vacancies, are not stable. This is evident from the defect configurations 4, 5, 6, and 19, where the calculated binding energies are all positive, indicating that the defect configurations are unstable. These results are not surprising, because substitutional krypton atoms introduce strain fields[49,50] in a titanium lattice, which may lead to lattice instability. Second, the presence of vacancies can stabilize the clusters. This is best illustrated in the case of defect configurations 4–6 ($p = 2; n = 0$), 7–9 ($p = 2; n = 1$). In these cases, the positive binding energies of the configurations without vacancies become negative (indicating stability) on the addition of a single vacancy to the krypton clusters. The influence of vacancies in the $p = 2$ cluster is further underlined if defect groupings ($p = 2; n = 1$) (defects 7–9), ($p = 2; n = 2$) (defects 10–12), and ($p = 2; n = 3$) (defects 13–15) are taken into consideration. Here, for the same number of krypton atoms, i.e., $p = 2$, increasing number of vacancies, n, results in increased stability. A similar trend is obtained for ($p = 10; n = 1, 7, 9$) (defects 20–22), although a systematic analysis of $p = 10$ compact clusters was not undertaken, owing to the huge number of possible configurations. This suggests that

TABLE II. Interaction energy characteristics of vacancy-krypton defect configurations in hcp titanium. n, p, and δE_v^{Kr}, respectively, represent number of vacancies, number of krypton atoms, and their interaction energies in eV. The calculations were done at constant volume using the 120-atom supercell described in the text.

Defect	n	p	$\delta E_v^{\mathrm{Kr}}/p$
1	0	1	–
2	1	1	−0.85
3	1	1	−0.93
4	0	2	1.14
5	0	2	1.21
6	0	2	1.63
7	1	2	−0.40
8	1	2	−0.74
9	1	2	−0.57
10	2	2	−1.38
11	2	2	−1.60
12	2	2	−1.28
13	3	2	−1.69
14	3	2	−1.72
15	3	2	−1.71
16	4	2	−1.33
17	4	2	−2.36
18	4	2	−1.72
19	0	11	1.24
20	1	10	−0.63
21	7	10	−2.14
22	9	10	−2.60

the binding energy per krypton atom increases with increasing number of vacancies. This observation may be explained by a simple physical argument: the presence of vacancies reduces the strain in the titanium lattice and this leads to increased stability of the defect cluster.

Next, we examine how the spatial distribution of vacancies determines the binding, and hence the relative stabilities of the defect complexes. Defect clusters 16 and 18 ($p = 2$; $n = 4$) have a greater number of vacancies than defect groupings 13–15 ($p = 2$; $n = 3$) for the same krypton atom configurations, yet the binding energy of the latter is either greater or approximately equal to the former, in contrast to our earlier conclusion. The reason is that the configurations of defects 16 and 18 are such that each of the krypton atoms is only able to interact maximally with two vacancies. This is in contrast to defect groupings 13–15, where each of the krypton atoms is positioned such that it is able to interact maximally with three vacancies. For the same reason, the binding energy of defect 17, which has the same krypton configuration and same vacancy-to-krypton ratio as defect 16, is almost double the binding energy of the latter defect: In defect 17, each of the two krypton atoms is at the closest distance to the vacancies, in addition to each krypton atom having a vacancy in the second nearest neighbor (in the same plane). Therefore, we may summarize the spatial effects of vacancy-krypton distributions as follows: for a given vacancy-to-krypton ratio in a cluster, greater cluster stability occurs when the krypton atoms interact optimally with the vacancies. This observation may be understood in terms of a strain-relief argument,

whereby the strain fields owing to krypton atoms are efficiently reduced when there are optimal interactions between the vacancies. Furthermore, defect configurations such as 16, 17, 18, 21, and 22 confirm the possibility of inert-gas atoms to nucleate in cavities created by vacancies in implanted metals.

C. Substitutional krypton migration

Next, we discuss the substitutional krypton atom migration. Substitutional krypton atoms may migrate in titanium via the vacancy or dissociation mechanisms. The vacancy mechanism involves the krypton atom exchanging sites with an adjacent vacancy, while the dissociation mechanism involves the krypton atom dissociating from its substitutional lattice position and migrating interstitially until it is trapped in another vacancy. Effective migration energies of substitutional krypton may be estimated depending on the concentration of vacancies in titanium. Of particular interest is the case of krypton energetically implanted into titanium at low or intermediate temperatures. In this case, implantation-induced vacancies may dominate over thermal vacancies, depending on implantation conditions, such as implanted krypton concentration or the implantation energy. The effective migration energy $E_{\mathrm{dis}}^{m,i}(\mathrm{Kr}_{\mathrm{subs}})$ for krypton diffusion by dissociation mechanism is then given by[51]

$$E_{\mathrm{dis}}^{m,i}(\mathrm{Kr}_{\mathrm{subs}}) = E^b(\mathrm{Kr}_{\mathrm{int}}, V) + E^m(\mathrm{Kr}_{\mathrm{int}}),$$

that is, the sum of the interstitial krypton-vacancy binding, $E^b(\mathrm{Kr}_{\mathrm{int}}, V)$, and the energy barrier for the interstitial krypton migration, $E^m(\mathrm{Kr}_{\mathrm{int}})$. Using $E^m(\mathrm{Kr}_{\mathrm{int}}) = 0.58$ eV (Ref. [27]) and $E^b(\mathrm{Kr}_{\mathrm{int}}, V) = 2.71$ eV, $E_{\mathrm{dis}}^{m,i}(\mathrm{Kr}_{\mathrm{subs}}) = 3.29$ eV. However, if thermal vacancies prevail, their concentration will be determined by the vacancy formation energy, E_f^v. In this case, the effective migration energy by dissociation mechanism, $E_{\mathrm{dis}}^{m,t}(\mathrm{Kr}_{\mathrm{subs}})$, will be given by[52]

$$E_{\mathrm{dis}}^{m,t}(\mathrm{Kr}_{\mathrm{subs}}) = E^b(\mathrm{Kr}_{\mathrm{int}}, V) + E^m(\mathrm{Kr}_{\mathrm{int}}) - E_f^v,$$

with $E_f^v = 1.92$ eV.[35] Therefore, in this case, $E_{\mathrm{dis}}^{m,t}(\mathrm{Kr}_{\mathrm{subs}}) = 1.37$ eV.

Next, we consider the migration of substitutional krypton via the vacancy mechanism. This corresponds to a krypton atom previously occupying a vacant lattice position migrating toward another vacancy. We first examine the relaxed configuration of substitutional krypton atom in the presence of a first- and second-neighbor vacancy. This is illustrated using configurations 2 and 3, respectively, in Fig. 2. Defect configuration 2 corresponds to a substitutional krypton separated from a vacancy in another plane (along the c direction) by ∼2.873 Å. In configuration 3, the substitutional krypton atom and the vacancy are in the same plane, and are separated by the lattice parameter $a = 2.930$ Å. The vacancy in configurations 2 and 3 thus constitute the first and second nearest neighbor to the krypton atom, respectively. After atomic relaxation, configuration 3 is slightly more stable with a negative vacancy to a substitutional krypton binding energy of 0.93 eV, compared to 0.85 eV for the configuration 2. The stability of the two configurations (cf. Table II) indicates that substitutional krypton can form a substitutional krypton-vacancy pair complex. In the relaxed
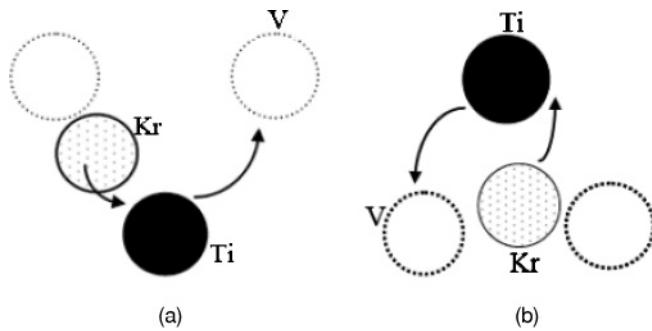
FIG. 4. Models showing (a) in-plane (top view) and (b) out-of-plane (side view) Kr-vacancy (*V*) migration via a vacancy exchange mechanism in hcp titanium.

krypton-vacancy complex for both configurations, the krypton atom sits asymmetrically between two neighboring vacant sites. Finally, we propose two major paths through which a krypton atom can migrate via the vacancy mechanism, as shown in Fig. 4. The first mechanism is an in-plane, two-dimensional migration process [shown in Fig. 4(a)], that is, the krypton and the vacancy are located in the same atomic plane. The migration is such that a nearby titanium atom moves toward the vacancy, while the krypton atom migrates to occupy the vacant site created by the migrating titanium atom. In this way, the krypton atom has migrated by an atomic distance, within a plane. The second mechanism [Fig. 4(b)] is an out-of-plane, three-dimensional migration process, and is such that the krypton atom migrates to another lattice plane. The titanium atom (located above the plane containing the krypton atom) nearest to the krypton moves to occupy the vacant position, while the krypton moves along the *c* direction to occupy the vacant site left by the titanium atom. Figures 5(a) and 5(b) show the migration barrier for the minimum paths. Relaxed configurations corresponding to the points marked on the figures are also shown in Figs. 6(a)–6(f). For the in-plane krypton migration, the first (*d*) and the last (*f*) images are equivalent and correspond to configuration 3 discussed above, hence their energies are equal, as shown in Fig. 5(a). Thereby, in image *f* the diffusing krypton is almost at half the distance between the two vacancies, while the migrating titanium atom is already occupying the normal lattice site. For the out-of-plane migration, the first and the last images correspond to configuration 2 and 3, respectively, and thus the first image is at slightly higher energy than the last image, as shown in Fig. 5(b). In image *c*, the diffusing krypton atom is almost at an octahedral position, midway between the vacancies, while the titanium atom is at a regular lattice site. The migration energy barrier for the in-plane migration is ∼0.94 eV, while for the out-of-plane migration, the barrier is ∼1.28 eV. These migration energy barriers are lower than the energy required to separate a vacancy from a substitutional krypton-vacancy complex, that is, 1.32 or 1.40 eV. The former is estimated from the sum of the vacancy migration energy, i.e., 0.47 eV, and the binding energy of vacancy to substitutional krypton for defect 2 (i.e., 0.85 eV, see Table II), while the latter is the sum of the same vacancy migration energy (0.47 eV) and the binding energy of vacancy to substitutional krypton for defect 3 (i.e., 0.93 eV, see Table II).
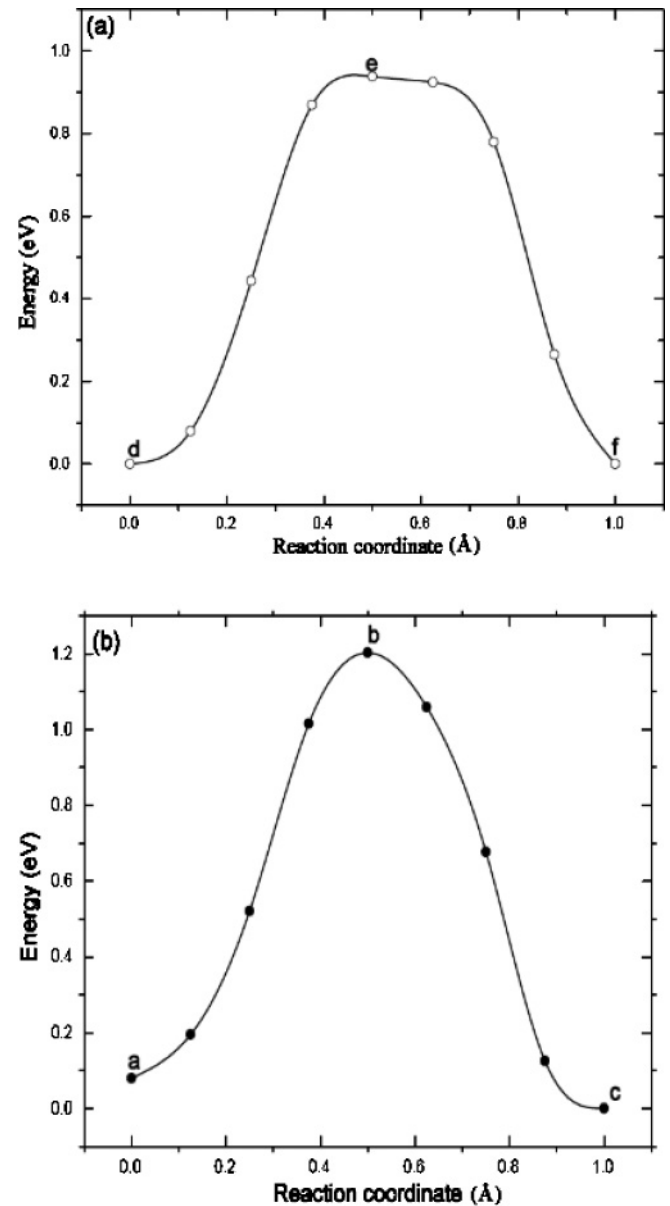

FIG. 5. Migration barrier for the (a) in-plane and (b) out-of-plane krypton diffusion via the vacancy mechanism.

It is therefore expected that the substitutional krypton-vacancy complex is able to migrate over an appreciable distance via substitutional krypton-vacancy mechanisms. The vacancy concentration C_v is thus increased by the amount of krypton-vacancy complexes, the concentration of which may be represented as

$$C_v \propto \exp\left[-\left(E_v^f + E_{KrV,V}^b\right)/kT\right],$$

where E_v^f and $E_{KrV,V}^b$ are the vacancy formation energy and vacancy-krypton binding energy, respectively. The mobility of the krypton-vacancy complex will give rise to an enhanced self-diffusion. It should be mentioned that other impurities atoms such as Fe, Ni, Co, and C, which are usually present,[53] albeit in small quantities, in high-purity polycrystalline metals, are fast interstitial diffusers. Therefore, when they form stable vacancy-interstitial impurity complexes, they also contribute
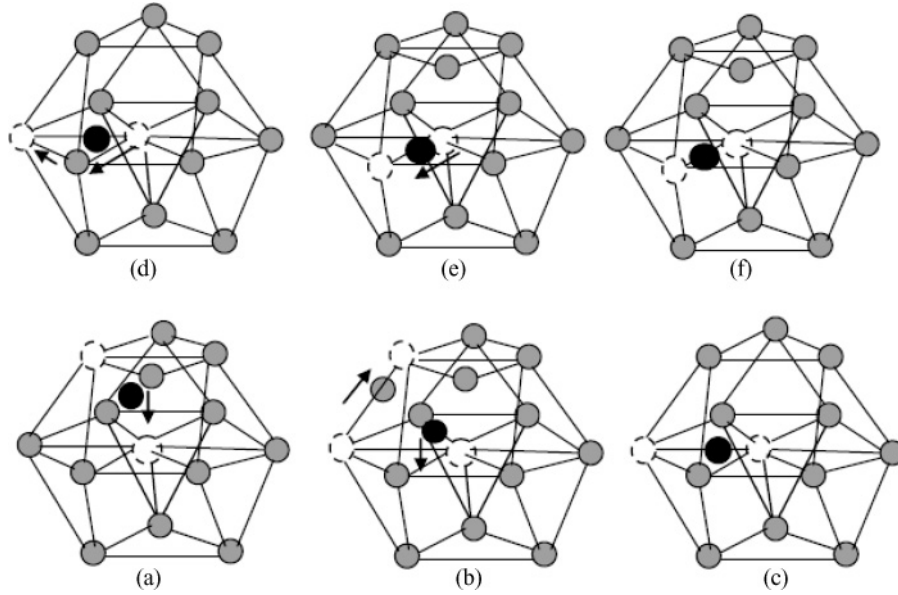
FIG. 6. Schematics representing the relaxed configurations for the images in the minimum energy path for substitutional krypton migration; (a)–(c) are the images for the out-of-plane migration, while (d)–(f) correspond to images for the in-plane migration. Black circles represent the krypton atoms, gray circles are the titanium atoms, and the open dotted circles represent vacancies.

to enhanced self-diffusion in the material. The presence of dislocations, twin bands, and other extended defects may result in residual stresses that also drive the point defects and thus contribute to enhanced self- and foreign-impurity defect diffusion.[10,54] It should be mentioned, however, that the direction of migration of defects is dependent on the preexisting stress profile in the material.[54,55] The enhanced diffusion coupled with the low migration barrier energy of divacancy may explain the observed multiple vacancies that form voids beyond the projected range in krypton-implanted hcp titanium. The voids introduce additional compressive stress deeper in the titanium sample.[16] Divacancies may also migrate and agglomerate with substitutional krypton-vacancy clusters to form inert-gas-filled cavities, which may serve as nucleation centers for nanoclusters of krypton atoms.

The effective activation energy for the substitutional krypton migration via the vacancy mechanism, when thermal vacancies dominate, is given by[52]

$$\Delta E_{\mathrm{vac}}^{m,t}(\mathrm{Kr}_{\mathrm{subs}}) = E_v^f - E_{\mathrm{Kr}V,V}^b + E_{\mathrm{Kr}V,V}^m,$$

where E_v^f is the formation energy of a single vacancy, $E_{\mathrm{Kr}V,V}^b$ its binding energy to a substitutional krypton atom, and $E_{\mathrm{Kr}V,V}^m$ is the migration energy for this complex. For in-plane migration, using $E_v^f = 1.92$ eV, $E_{\mathrm{Kr}V,V}^b = 0.93$ eV, and $E_{\mathrm{Kr}V,V}^m = 0.94$ eV, one obtains $\Delta E_{\mathrm{vac}}^{m,t}(\mathrm{Kr}_{\mathrm{subs}}) = 1.93$ eV. For the out-of-plane migration, the effective migration energy is higher, i.e., 2.27 eV. However, if implantation-induced vacancies prevail, the effective migration barrier for the krypton diffusion via the vacancy mechanism is given by[52]

$$\Delta E_{\mathrm{vac}}^{m,i}(\mathrm{Kr}_{\mathrm{subs}}) = E_{\mathrm{Kr}V,V}^m - E_{\mathrm{Kr}V,V}^b.$$

Using $E_{\mathrm{Kr}V,V}^m = 1.28$ eV and $E_{\mathrm{Kr}V,V}^b = 0.85$ eV for the out-of-plane migration, one obtains $\Delta E_{\mathrm{vac}}^{m,i}(\mathrm{Kr}_{\mathrm{subs}}) = 0.43$ eV. As for the in-plane migration, the effective migration energy is ∼0.1 eV. If $\Delta E_{\mathrm{vac}}^{m,t}(\mathrm{Kr}_{\mathrm{subs}}) = 1.93$ eV (for the in-plane migration) or 2.27 eV (for the out-plane migration)

is compared with $\Delta E_{\mathrm{dis}}^{m,t}(\mathrm{Kr}_{\mathrm{subs}}) = 1.37$ eV, we may conclude that if thermal vacancies dominate after implantation, the dissociation mechanism is expected to be dominant. However, if implantation-induced vacancies dominate, the vacancy concentration depends on the initial implantation conditions, and therefore no general conclusion may be drawn. Nevertheless, we may speculate, based on the calculated effective migration energy, $\Delta E_{\mathrm{vac}}^{m,i}(\mathrm{Kr}_{\mathrm{subs}}) = 0.43$ eV (out-of-plane migration) or 0.1 eV (in-plane migration) and $\Delta E_{\mathrm{dis}}^{m,i}(\mathrm{Kr}_{\mathrm{subs}}) = 3.29$ eV, that krypton diffusion will proceed via the vacancy mechanism. Experimentally, the actual diffusion mechanism governing krypton migration after implantation may be determined from thermal desorption experiments[7] or thermal extraction mass spectrometry.[55]

IV. CONCLUSION

To summarize, we have performed first-principles calculations to determine the migration of vacancy and divacancy in hcp titanium. Divacancy was found to have a lower migration energy barrier as compared to a monovacancy. We have also studied the energetics and stability of clusters of krypton impurities and vacancies. We have shown that substitutional krypton clusters are not stable, but are stabilized by vacancies. The strength of the stability was found to depend on the vacancy-krypton ratio, and on the spatial distribution of the vacancies. The influence of vacancies on the cluster stability has been explained by simple strain-relief arguments, whereby the strain associated with krypton atoms clusters may be relieved by agglomerating vacancies. Furthermore, we have investigated the migration of substitutional krypton. It was shown that substitutional krypton migration proceeds via the vacancy mechanism, if implantation-induced vacancies dominate the postimplantation process. On the other hand, if thermal vacancies prevail, krypton atom migration proceeds via the dissociation mechanism. The low migration barrier energy of the divacancy, coupled with enhanced diffusion of stable krypton-vacancy pairs, implies that vacancies are able to diffuse fast and cluster to form larger defects, such

as voids, which may introduce additional compressive stress deeper in the sample, as observed in a related experiment. Furthermore, divacancies may agglomerate with substitutional krypton-vacancy complexes to form inert-gas-filled cavities, which may exhibit unusual electronic and optical properties.

*abdulrafiu.raji@uct.ac.za

[1] K. Iakoubovskii, K. Mitsuishi, and K. Furuya, Phys. Rev. B **78**, 064105 (2008).

[2] R. C. Birtcher, S. E. Donnelly, M. Song, K. Furuya, K. Mitsuishi, and C.W. Allen, Phys. Rev. Lett. **83**, 1617 (1999).

[3] S. E. Donnelly, R. C. Birtcher, C .W. Allen, I. Morrison, K. Furuya, M. H. Song, K. Mitsuishi, and U. Dahmen, Science **296**, 507 (2002).

[4] S. E. Donnelly, Radiat. Eff. **90**, 1 (1985).

[5] A. Anderman and W. G. Gehman, Phys. Status Solidi **30**, 283 (1968).

[6] D. T. Britton, F. P. Nemalili, and M. Härting, Phys. Status Solidi **198**, 238 (2003).

[7] R. Vassen, H. Trinkaus, and P. Jung, Phys. Rev. B **44**, 4206 (1991).

[8] K. O. Jensen, M. Eldrup, N. J. Pedersen, and J. H. Evans, J. Phys. F **18**, 1703 (1988).

[9] A. vom Felde, J. Fink, Th. Müller-Heinzerling, J. Pflüger, B. Scheerer, G. Linker, and D. Kaletta, Phys. Rev. Lett. **53**, 922 (1984).

[10] M. Härting, M. Yaman, R. Bucher, and D. T. Britton, Adv. Eng. Mater. **4**, 592 (2002).

[11] P. Hohenberg and W. Kohn, Phys. Rev. **136**, B864 (1964).

[12] W. Kohn and L. J. Sham, Phys. Rev. **140**, A1133 (1965).

[13] C. Domain and C. S. Becquart, Phys. Rev. B **71**, 214109 (2005).

[14] L.Yang, X. T. Zu, and F. Gao, Physica B **403**, 2719 (2008).

[15] C. S. Becquart and C. Domain, Nucl. Instrum. Methods B **255**, 23 (2007).

[16] M. Härting, S. Nseygiyumva, A. T. Raji, G. Dollinger, P. Sperr, S. R. Naidoo, T. E. Derry, C. E. Comrie, and D. T. Britton, Surf. Coat. Technol. **201**, 8237 (2007).

[17] F. El-Mellouhi and N. Mousseau, Appl. Phys. A **86**, 309 (2007).

[18] L. Fedina, O. I. Lebedev, G. Van Tendeloo, J. Landuyt, O. Mironov, and E. H. C. Parker, Phys. Rev. B **61**, 10336 (2000).

[19] H. Trinkaus, B. N. Singh, and S. I. Golubov, J. Nucl. Mater. **283-287**, 89 (2000).

[20] W. E. Pickett, Comput. Phys. Rep. **9**, 115 (1989).

[21] G. Henkelman and H. Jónsson, J. Chem. Phys. **113**, 9978 (2000).

[22] W. Y. Hu, B. W. Zhang, B. Y. Huang, F. Gao, and D. J. Bacon, J. Phys. Condens. Matter **13**, 1193 (2001).

[23] W. O. Hofer, K. Besocke, and B. Stritzker, Appl. Phys. A **30**, 83 (1983).

[24] A. Norman, Radiat. Res. Suppl. **7**, 33 (1967).

[25] Y. Matsukawa and S. J. Zinkle, Science **318**, 959 (2007).

[26] E. Yagi, M. Iwaki, K. Tanaka, I. Hashimoto, and H. Yamaguchi, Nucl. Instrum. Methods B **33**, 724 (1988).

[27] A. T. Raji, S. Scandolo, R. Mazzarello, S. Nsengiyumva, M. Härting, and D. T. Britton, Nucl. Instrum. Methods B **267**, 2991 (2009).

[28] K. Furuya, K. Mitsuishi, M. Song, and T. Saito, in *Proceedings of International Conference on Ion Implantation Technology* (IEEE, Piscataway, NJ, 1999), Vol. 2, p. 811.

[29] M. Song, K. Mitsuishi, H. Yasuda, and K. Furuya, J. Electron. Microsc. **51**, S211 (2002).

[30] S. Scandolo, P. Giannozzi, C. Cavazzoni, S. Gironcoli, A. Pasquarello, and S. Baroni, Z. Kristallogr. **220**, 574 (2005).

[31] P. Giannozzi *et al.*, J. Phys. Condens. Matter **21**, 395502 (2009).

[32] J. P. Perdew, J. A. Chevary, S. H. Vosko, K. A. Jackson, M. R. Pederson, D. J. Singh, and C. Fiolhais, Phys. Rev. B **46**, 6671 (1992); **48**, 4978 (1993).

[33] D. Vanderbilt, Phys. Rev. B **41**, R7892 (1990); G. Kresse and J. Hafner, J. Phys. Condens. Matter **6**, 8245 (1994).

[34] M. Methfessel and A. T. Paxton, Phys. Rev. B **40**, 3616 (1989).

[35] A. T. Raji, S. Scandolo, R. Mazzarello, S. Nsengiyumva, M. Härting, and D. T. Britton, Philos. Mag. **89**, 1629 (2009).

[36] L. Tsetseris, N. Kalfagiannis, S. Logothetidis, and S. T. Pantelides, Phys. Rev. B **76**, 224107 (2007).

[37] F. Willaime, A. Satta, M. Nastar, and O. Le Bacq, Int. J. Quantum Chem. **77**, 927 (2000).

[38] G. M. Hood, H. Zou, D. Gupta, and R. J. Shultz, J. Nucl. Mater. **223**, 122 (1995).

[39] A. M. Monti and E. J. Savino, Phys. Rev. B **23**, 6494 (1981).

[40] R. R. Zope and Y. Mishin, Phys. Rev. B **68**, 024102 (2003).

[41] J. R. Fernández, A. M. Monti, and R. C. Pasianot, J. Nucl. Mater. **229**, 1 (1996).

[42] C. M. Libanati and S. F. Dyment, Acta Metall. **11**, 1263 (1963).

[43] M. Köppers, C. Herzig, M. Friesel, and Y. Mishin, Acta Mater. **45**, 4181 (1997).

[44] R. A. Johnson, Philos. Mag. A **63**, 865 (1991).

[45] R. A. Johnson and J. R. Beeler, in *Interatomic Potentials and Crystalline Defects*, edited by J. K. Lee (The Metallurgical Society AIME, New York, 1981), p. 165.

[46] C. Domain and C. S. Becquart, Phys. Rev. B **71**, 214109 (2005).

[47] D. A. Anderson and S. I. Simak, Phys. Rev. B **70**, 115108 (2004).

[48] K. Nordlund and R. S. Averback, Phys. Rev. Lett. **80**, 4201 (1998).

[49] D. T. Britton and M. Harting, Adv. Eng. Mater. **4**, 629 (2002).

[50] J. D. Eshelby, Philos. Trans. R. Soc. London A **244**, 87 (1951).

[51] V. Sciani and P. Jung, Radiat. Eff. **78**, 87 (1983).

[52] C-C. Fu and F. Willaime, Phys. Rev. B **72**, 064117 (2005).

[53] M. Behar, F. Dyment, R. A. Perez, J. H. R. Dos Santos, R. L. Maltez, and E. J. Savino, Philos. Mag. A **63**, 967 (1991).

[54] W. G. Wolfer and M. Ashkin, Scr. Metall. **7**, 1175 (1973).

[55] K. Takaishi, T. Kikuchi, K. Furuya, I. Hashimoto, H. Yamaguchi, E. Yagi, and M. Iwaki, Phys. Status Solidi A **95**, 135 (1986).